Posted on Authorea 4 Aug 2020 — The copyright holder is the author/funder. All rights reserved. No reuse without permission. — https://doi.org/10.22541/au.159654396.62738949 — This a preprint and has not been peer reviewed. Data may be preliminary.

Sampling Error of Continuous Periodic Data and its Application for Geodesy

Lorant Foldvary[1]

[1]Obuda University

August 4, 2020

Abstract

Data acquisition for geoinformatics cannot be done continuously, but by discrete sampling of the object or phenomenon. The sampling involves errors on the knowledge of the continuous signal due to the loss of information in the sampling procedure. In the present study, an analytical formulation of the sampling error is provided, which embodies the amplitude, phase, bias and periodicity of the sampling error. The analysis is then subsequently applied for case studies: for the GRACE and GRACE-FO monthly solutions, and for different realizations of the Hungarian Gravimetric Network.

Introduction

Data acquisition for geoinformatics contains collection of spatially and/or temporally changing features, which are continuous by nature. No data acquisition can be done continuously, but by discrete sampling of the phenomenon. Discrete sampling is often then considered to be uninterrupted sequences of continuous data, which results in an underestimation of the actual signal.

Shannon's proof (Shannon 1949, 1998) on the sampling theorem illustrates elegantly the feasibility of recovering: while sampling of a band-limited signal means a multiplication of the continuous signal with Dirac impulses in the time domain, in the frequency domain (due to the corresponding convolution) it yields repetition of the spectrum of the original function. Therefore, theoretically the original function can be recovered perfectly by filtering the sampled signals spectrum to the original bands, which means a multiplication in the frequency domain with a boxcar window of the proper size (see e.g. Chapter 3 of Marks 1991). This approach is, however, too idealized, as it assumes a band limited signal, while real signals are never exactly bandlimited, but there always an aliasing is observed. Also, in practice no ideal anti-aliasing low-pass filters can be constructed (Unser 2000). (For details on related issues of the sampling theory, the reader is referred to Marks (1991, 1993) and Unser (2000)).

In fact, in practice Shannon's formulation is rarely used, as sinc function (the time domain equivalent of the boxcar filtering) decays slowly. For the practice, in case of an 'appropriately' sampled signal, intermediate values are assumed to be determined with 'appropriate' accuracy by linear interpolation. (Accordingly, the present study also assumes that the sampled signal is approximated by linear interpolation). Still, the relevance of Shannon's theorem is essential, as (theoretically) any signal can be interpreted as infinite number of periodic signals as Fourier transformation provides such a decomposition.

$f(t) = \sum_{c=0}^{\infty} A_c sin(2\pi f_c t + \phi_c)$ (1)

Certainly, in practice no full equivalence of the original and the Fourier transform signals can be achieved as the transformation can make use of only finite numbers of frequencies, and also due to numerical limitations. Following, however, the idealization of Shannon, in this study, the effect of sampling is discussed for a

Posted on Authorea 4 Aug 2020 — The copyright holder is the author/funder. All rights reserved. No reuse without permission. — https://doi.org/10.22541/au.159654396.62738949 — This a preprint and has not been peer reviewed. Data may be preliminary.

discretization procedure with no error, and assuming no observation errors as well. Also, implicitly we assume the feasibility of (1), thus the discussion focus on periodic signals only. Note also, that in the practice of geoinformatics and Remote Sensing the discretization is often obtained by averaging over a finite segment of the data, e.g. Digital Terrain Models (DTM) are determined based on several observations referring to a certain pixel, resulting in aliasing the point-wise data by the block averaging (Földváry 2015). This study assumes perfectly point-wisely sampled data.

Nowadays, sampling algorithms are generalizing the Shannonian approach: instead of constraining the signal into a limited bandwidth before recovering it, the proper band-limited filter can be achieved by methods applying orthogonal, frequency dependent base functions, such as wavelets (Strang-Nguyen 1996; Mallat 1998), finite elements (Strang 1971; Selesnick 1999), frames (Duffin-Schaeffer 1952; Benedetto 1992), among others.

In summary, the aim of the study is to provide a mathematical tool for sampling error estimation. The sampling, by its discrete characteristics involves errors on the knowledge of the real continuous phenomenon. Without understanding the limitations of the discretization, the observed phenomenon may be interpreted falsely. In the present study, analytical formulation of the sampling error is to be provided, which embodies the characteristics of the sampling error by determining its amplitude, phase, bias and periodicity. Such information can be used for planning optimal resolution of sampling a process but cannot be used (and it is not the scope of this study) for reconstructing the original signal.

Formulation

Figure 1 displays an example of a periodic signal, which is sampled with a certain sampling period. Let T refer to the period of the signal, and T to the sampling period. If the sampling period is sufficiently fine, then the signal can efficiently be approximated by assuming linearity between two consecutive points. In practice, for sake of simplicity, such a linearity is assumed; accordingly, linear interpolation is used for approximating inner values of the signal.

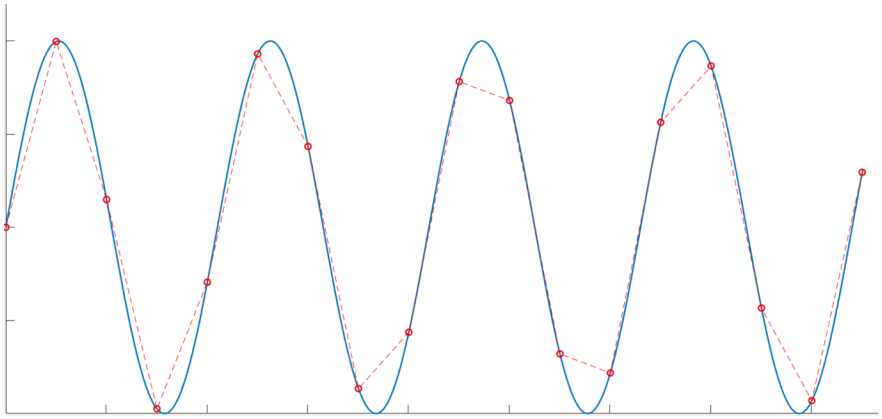


Figure 1. Sampled signal is approximated by linear interpolation. (The periodic signal is represented by the blue curve, the sampled values are red circles, and the linearly interpolated signal is the red dashed line).

Assume that the periodic signal with a period of T (equivalently can be described by its frequency, $\omega = 1/T$) is sampled regularly by a constant sampling rate, $T = 1/f_s$, where f_s is the sampling frequency. The dimension of the signal may range at different scales, even the content of the signal can be different, e.g. time in seconds, hours, years, ages or length in mm, m, km, AU. Therefore, instead of discussing actual reliable scales and magnitudes, in the present analysis the periodic function is characterized by its amplitude, A and frequency, ω, while the sampling is defined by the sampling rate, T, or equivalently by the ratio of the frequency of the signal, ω and the observation, f_s

Posted on Authorea 4 Aug 2020 — The copyright holder is the author/funder. All rights reserved. No reuse without permission. — https://doi.org/10.22541/au.159654396.62738949 — This a preprint and has not been peer reviewed. Data may be preliminary.

$N = \frac{\omega}{f_s} = \frac{T}{T}$ (2).

The amplitude, A is set arbitrarily to a unit, and error estimation due to the sampling is performed by considering two parameters: the frequency, ω of the signal and the ratio N. The error estimates are provided in percentage of the amplitude, A. Beyond$A$, ω and N, also the phase of the signal, ϕ is used for defining the periodic signal, however the calculus later is performed independently of this variable. All in all, the periodic function is defined as

$f(x) = Asin(2\pi\omega\ x + \phi)$ (3),

where x is the independent variable. The sampling affects the knowledge of the observed signal between the sampling epochs. Therefore, sampling error is modelled here as the difference of real and the (linearly) interpolated values. According to Figure 2, when the function value at an arbitrary epoch, x_k falling into the interval of $[x_i\ , x_{i+1}\ ]$, the error due to the sampling becomes the difference of the real, $f(x_k)$ and the interpolated, $f_{int}(x_k)$ function values, ε_k.

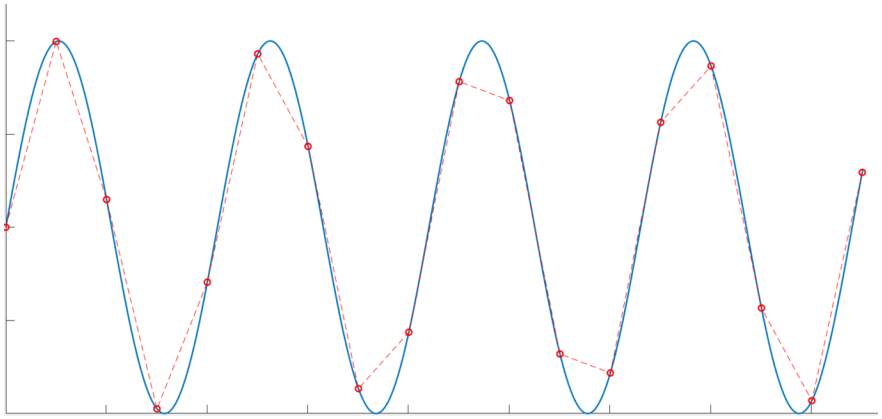


Figure 2. Errors due to sampling a periodic signal and approximating by linear interpolation

The interpolated function value,$f_{int}(x_k)$ can be derived by considering it as a point of division, i.e. it divides in a ratio of$(x_k\text{-}x_i)$:$(x_{i+1}\text{-}x_k)$ the join of points $(x_i\ ,\ f(x_i)\ )$ and $(x_{i+1}\ ,\ f(x_{i+1})\ )$:

$f_{\text{int}}\,(x_k) = \frac{(x_{i+1}-x_k)f(x_i)+(x_k-x_i)f(x_{i+1})}{x_{i+1}-x_i}$(4).

Accordingly, the sampling error at this epoch becomes

$\varepsilon_k = f\,(x_k) - f_{\text{int}}\,(x_k) = f(x_k) - \frac{(x_{i+1}-x_k)f(x_i)+(x_k-x_i)f(x_{i+1})}{x_{i+1}-x_i}$(5).

Note that the difference of two consecutive abscissae (in the denominator of the second term of the righthand side) is the sampling interval, $T = x_{i+1} - x_i$.

Generally, the sampling error in the engineering practice is estimated by L2-norm; for some applications also L1-norm and L-norm is used. The present study focuses on the L2-norm, which is derived after the simpler form of L1-norm. The L1-norm of the sampling error over the $[x_i\ ,\ x_{i+1}\ ]$ interval can be defined as it is the mean of the ε differences at all epochs, i.e.

$\sigma_{L1}\,([x_i, x_{i+1}]) = \frac{L1([x_i,x_{i+1}])}{n} = \frac{\sum_{x_i}^{x_{i+1}}|\varepsilon_k|}{n} = \frac{\int_{x_i}^{x_{i+1}}|\varepsilon(x)|\mathrm{dx}}{T}$(6).

The integral provides the area between the real and interpolated curves, which is then subsequently divided by the sampling interval. By rigorous calculus, a closed-form for the L1-norm (inserting (3) and (5) to (6)) can be derived by solving the definite integral of

Posted on Authorea 4 Aug 2020 — The copyright holder is the author/funder. All rights reserved. No reuse without permission. — https://doi.org/10.22541/au.159654396.62738949 — This a preprint and has not been peer reviewed. Data may be preliminary.

$$\sigma_{L1}\left([x_i, x_{i+1}]\right) = \frac{\int_{x_i}^{x_{i+1}} \left| Asin(2\pi\omega\ x+\phi) - \frac{(x_{i+1}-x)Asin(2\pi\omega\ x_i+\phi)+(x-x_i)Asin(2\pi\omega\ x_{i+1}+\phi)}{T} \right| \mathrm{dx}}{T} (7),$$

resulting in

$$\sigma_{L1}\left([x_i, x_{i+1}]\right) = |C \bullet \cos\left(2\pi\omega x_i + \phi\right) + S \bullet sin(2\pi\omega x_i + \phi)| (8),$$

where

$$C = \frac{A}{2\pi\omega T} - \frac{A}{2} sin(2\pi\omega T) - \frac{A}{2\pi\omega T} \cos\left(2\pi\omega T\right) (9)$$

and

$$S = -\frac{A}{2} + \frac{A}{2\pi\omega T} \sin\left(2\pi\omega T\right) - \frac{A}{2} cos(2\pi\omega T) (10).$$

For details of deriving (8), see Appendix A. By introducing the following notation

$$n = 2\pi N = 2\pi\omega T\ (11)$$

it simplifies to

$$C = \frac{A}{n} - \frac{A}{2} sin(n) - \frac{A}{n} \cos\left(n\right) (12)$$

and

$$S = -\frac{A}{2} + \frac{A}{n} \sin\left(n\right) - \frac{A}{2} cos(n) (13).$$

Using the$C \bullet \cos\left(\alpha\right) + S \bullet \sin\left(\alpha\right) = R \bullet \sin\left(\alpha + \varphi\right)$conversion, the parameters C and S can be replaced to R andϕ as

$$\sigma_{L1}\left([x_i, x_{i+1}]\right) = R \bullet |sin(2\pi\omega x_i + \phi + \varphi)| (14),$$

where

$$R = \sqrt{2}\frac{A}{n}\sqrt{\left(1 + \frac{n^2}{4}\right) - nsin(n) - \left(1 - \frac{n^2}{4}\right)\cos\left(n\right)} (15)$$

and

$$\varphi = arctg\frac{1 - \frac{n}{2}\sin(n) - cos(n)}{-\frac{n}{2} + \sin(n) - \frac{n}{2}cos(n)} (16).$$

Note that (15) and (16) depends purely on the ratio of the sampling interval and the period of the signal, N, c.f. (11). In (15) it is also multiplied by A, which provides the scale (and the unit) of$R$, i.e. it works as the scale factor of the ordinate of the figure, while only the ratio N is relevant along the abscissa.

Similarly, the sampling error based on the L2-norm can also be derived applying the definition of RMS,

$$\sigma_{L2}\left([x_i, x_{i+1}]\right) = \frac{L2([x_i, x_{i+1}])}{\sqrt{n}} = \sqrt{\frac{\sum_{x_i}^{x_{i+1}} {\varepsilon_k}^2}{n}} = \sqrt{\frac{\int_{x_i}^{x_{i+1}} \varepsilon(x)^2 \mathrm{dx}}{T}} (17).$$

Making use of (3) and (5), the definite integral in (17) becomes

$$L2\left([x_i, x_{i+1}]\right)^2 =$$

$$\int_{x_i}^{x_{i+1}} \left(Asin(2\pi\omega\ x + \phi) - \frac{(x_{i+1}-x)Asin(2\pi\omega\ x_i+\phi)+(x-x_i)Asin(2\pi\omega\ x_{i+1}+\phi)}{T} \right)^2 \mathrm{dx} (18),$$

following similar steps of derivation to Appendix A, it can be expressed in a compact form of

$$L2\left([x_i, x_{i+1}]\right)^2 = C \bullet \cos\left(4\pi\omega x_i + 2\phi\right) + S \bullet \sin\left(4\pi\omega x_i + 2\phi\right) + B (19),$$

where

$$C = -\frac{A^2 T}{24\pi^2\omega^2 T^2} \left\{ 4\pi^2\omega^2 T^2 - 6 + \left(4\pi^2\omega^2 T^2 - 6\right)\cos\left(4\pi\omega T\right) + \left(4\pi^2\omega^2 T^2 + 12\right)\cos\left(2\pi\omega T\right) - 9\pi\omega T sin(4\pi\omega T) \right\}$$

Posted on Authorea 4 Aug 2020 — The copyright holder is the author/funder. All rights reserved. No reuse without permission. — https://doi.org/10.22541/au.159654396.62738949 — This a preprint and has not been peer reviewed. Data may be preliminary.

(20),

$$S = -\frac{A^2T}{24\pi^2\omega^2T^2}\left\{9\pi\omega T - \left(4\pi^2\omega^2T^2 - 6\right)\sin\left(4\pi\omega T\right) - \left(4\pi^2\omega^2T^2 + 12\right)\sin\left(2\pi\omega T\right) - 9\pi\omega T cos(4\pi\omega T)\right\}$$

(21),

and

$B = -\frac{A^2T}{24\pi^2\omega^2T^2}\left\{12 - 20\pi^2\omega^2T^2 - \left(4\pi^2\omega^2T^2 + 12\right)\cos\left(2\pi\omega T\right)\right\}$(22).

By introducing the n defined by (11), it simplifies to

$$C = -\frac{A^2T}{6n^2}\left\{n^2 - 6 + \left(n^2 - 6\right)\cos\left(2n\right) + \left(n^2 + 12\right)\cos\left(n\right) - \frac{9}{2}nsin(2n)\right\}$$

(23),

$$S = -\frac{A^2T}{6n^2}\left\{\frac{9}{2}n - \left(n^2 - 6\right)\sin\left(2n\right) - \left(n^2 + 12\right)\sin\left(n\right) - \frac{9}{2}ncos(2n)\right\}$$

(24),

and

$B = -\frac{A^2T}{6n^2}\left\{12 - 5n^2 - \left(n^2 + 12\right)\cos\left(n\right)\right\}$(25).

Using the$C \bullet \cos\left(\alpha\right) + S \bullet \sin\left(\alpha\right) = R \bullet \sin\left(\alpha + \varphi\right)$conversion, the parameters C and S can be replaced to R andφ as

$L2\left(\left[x_i, x_{i+1}\right]\right)^2 = R \bullet \sin\left(4\pi\omega x_i + 2\phi + \varphi\right) + B$(26),

where

$R = \frac{A^2T}{6n^2}\left(\left(n^2 + 12 - 9n\sin\left(n\right) + \left(2n^2 - 12\right)\cos\left(n\right)\right)^2\ (n) + \frac{1}{4}\left(-9n + 9n\cos\left(2n\right) + \left(2n^2 - 12\right)\sin\left(2n\right) + \left(2n^2 + 24\right)\sin\left(n\right)\right)^2\right.$

(27),

$\varphi = arctg\frac{n^2-6+\left(n^2-6\right)\cos(2n)+\left(n^2+12\right)\cos(n)-\frac{9}{2}nsin(2n)}{\frac{9}{2}n-\left(n^2-6\right)\sin(2n)-\left(n^2+12\right)\sin(n)-\frac{9}{2}ncos(2n)}$(28)

and B is as in (25). As (23) to (28) refers to$L2\left(\left[x_i, x_{i+1}\right]\right)^2$, the sampling error can be determined by (17) as

$\sigma_{L2}\left(\left[x_i, x_{i+1}\right]\right) = \frac{L2\left(\left[x_i, x_{i+1}\right]\right)}{\sqrt{T}} = \sqrt{\frac{L2\left(\left[x_i, x_{i+1}\right]\right)^2}{T}} = \sqrt{\frac{R\bullet\sin(4\pi\omega x_i+2\phi+\varphi)+B}{T}}$(29),

so no closed-form solution can be derived. Similarly to (15) and (16), (27) and (28) depends purely on the ratio of the sampling interval and the period of the signal, N, and the amplitude, R provides the scale and the unit in (27) by the multiplicator of A^2T.

Generalization of the formulation

A major shortcoming of the derived formulation is that it holds for purely periodic signal, which is indeed unrealistic. Note, however, that theoretically it can be generalized to any time series, as a Fourier series representation of a function consists of infinite number of periodic components, c.f. equation (1), where summation is done by$c$, and the reciprocal of any wavelengths,T_c , is the frequency,$f_c = \frac{1}{T_c}$. Due to the orthonormality of the Fourier base functions, the effect if the sampling error can be estimated to each component independently along the Fourier spectrum. Considering the frequency of a Fourier component of

Posted on Authorea 4 Aug 2020 — The copyright holder is the author/funder. All rights reserved. No reuse without permission. — https://doi.org/10.22541/au.159654396.62738949 — This a preprint and has not been peer reviewed. Data may be preliminary.

the signal, f_c and that of the sampling, f_s, the ratio N for each component can be determined similarly to equation (2):

$N_c = \frac{f_c}{f_s} = \frac{T}{T_c}$ (30).

It can then be used for each Fourier components independently using the equations of section 2.

Note that the bias does not need special attention in this case. As for the *c=0* term the Fourier component $T_0 = \infty$ and $f_0 = 0$, for any non-zero sampling frequency, $f_s \neq 0$, equation (30) becomes zero. For such a case, equations (11) to (16) and (23) to (29) has singularity, therefore the signal should be unbiased before estimating the sampling error.

Discussion

When sampling error of a periodic signal is to be estimated, it should definitely be kept in mind that it highly depends on which part of the signal it takes place, c.f. in Figure 1 the errors are apparently larger at the extremes (peaks) than around the inflection points.

Equations (8) to (10) and (19) to (22) provide analytic formulations for the periodicity of the sampling error. These equations indicate that it purely depends on the ratio of the signal period and the sampling interval, N. The periodicity of the sampling error is displayed in Figure 3 for an arbitrary example of N=0.05 ratio, i.e. 20 samplings during a period. It shows that the periodicity of the error is tied to the periodicity of the signal, but with a phase lag (it is 9° in this example). It also shows that for such a case the maximal error is 0.82% and 0.90% of the amplitude of the period of the signal, respectively for the L1 and L2 norms.

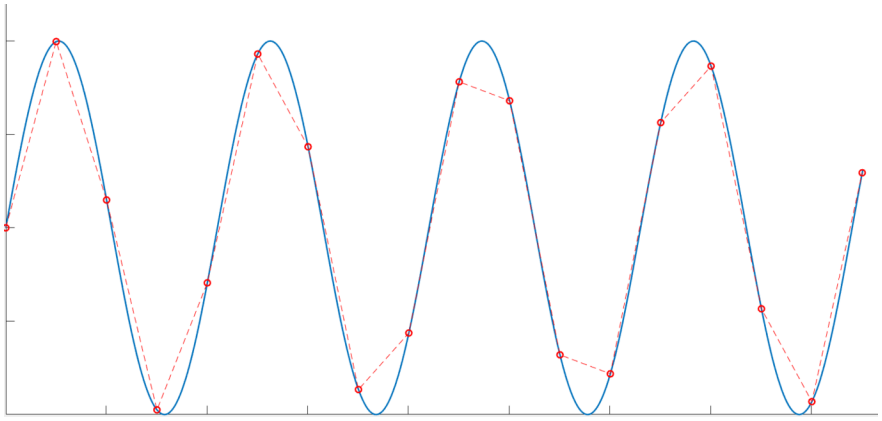


Figure 3. Sampling error due of a periodic signal with N=0.05 ratio.

The L1-norm and the L2-norm based sampling errors are shown in Figure 4 for a range of N ratios in the interval of [0.01, 0.5]. The limits were chosen considering practical aspect. The tested finest resolution was 0.01 (equivalent to 10 samplings per each period), which has resulted in negligible, 0.03% and 0.04% errors using the L1-norm and the L2-norm, respectively. The tested largest ratio was chosen in accordance with the Nyquist criterion, which says that meaningful frequency components of the properly sampled periodic signal exist below the half of the period of the signal, i.e. the Nyquist frequency (see e.g. Leis, 2011). For this extreme case, the sampling error was found to be 63.7% and 70.7% for the L1-norm and the L2-norm, respectively.

Posted on Authorea 4 Aug 2020 — The copyright holder is the author/funder. All rights reserved. No reuse without permission. — https://doi.org/10.22541/au.159654396.62738949 — This a preprint and has not been peer reviewed. Data may be preliminary.

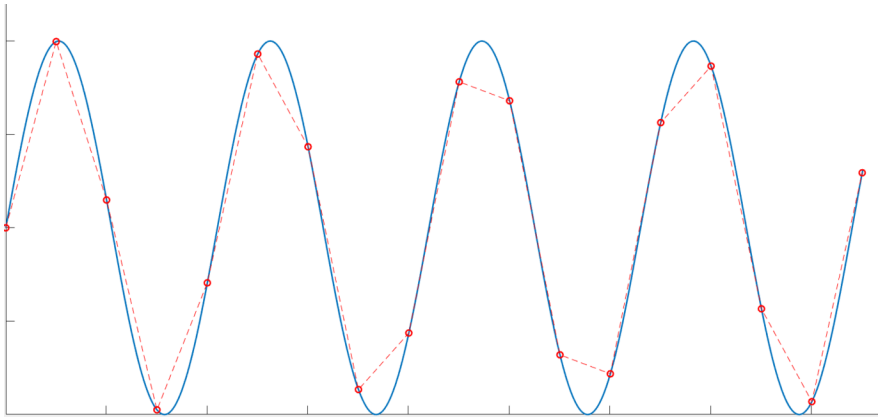


Figure 4. Sampling error for ratios ranges from 0.01 to 0.5.

Example in the time domain: GRACE monthly solutions

Temporal variations of the gravity field globally are monitored by the GRACE (between 2002-2017) and the GRACE-FO (from 2018) missions (Bettadpur, 2007). Mass variation in the Amazonas basin is dominated by the annual period of the hydrological cycle (c.f. gravity anomaly time series from GRACE and GRACE-FO monthly solutions in Figure 5). The monthly sampling is equivalent to N=1/12=0.083. Using (14) and (29), the maximal L1-norm sampling error becomes 2.27%, while the maximal L2-norm error is 2.49%.

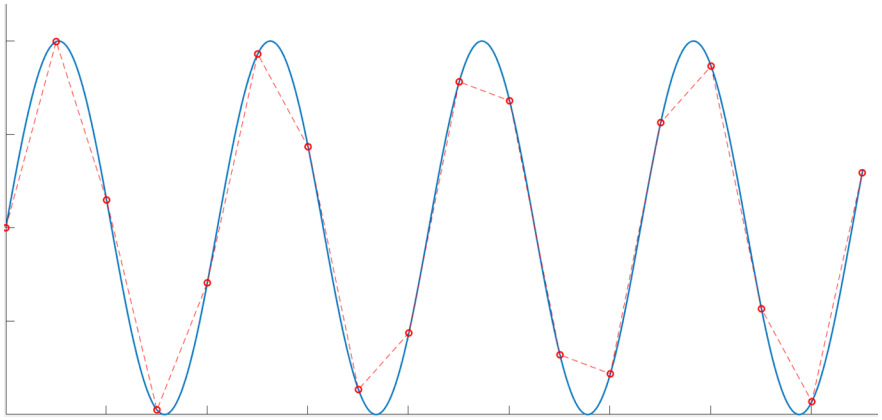


Figure 5. Gravity anomaly in the Amazonas basin using GRACE and GRACE-FO monthly solutions.

According to Földváry (2015), the annual amplitude is underestimated due to the averaging over the sampling period by 1.15%, thus the effect of the sampling error exceeds this phenomenon. Nevertheless, the GRACE and GRACE-FO models notably scatter from the annual characteristics (c.f. Figure 5, where also a best fit annual and semiannual curve is presented). The deviations of the detrended and unbiased GRACE/GRACE-FO monthly gravity anomalies from an annual and semiannual periodic curve is 35.58% of the magnitude of the signal, in average. This deviation consists of non-periodic signal, modelling errors (such as errors of the atmospheric correction, leakage of signal from outside of the basin, errors of smoothing and de-correlation filtering) and observation errors (integrating such errors as system-noise error in the KBR range-rate measurements, accelerometer error, errors of the ultra-stable oscillator, and orbit errors) as well (Swenson et al., 2003). Considering that the errors of GRACE are believed to be largely free of annual components (Wahr et al., 2006), the estimated annual component on Figure 5 can be considered to be purely due to the

annual variations of the total water storage, consequently, it can be considered to be a real signal, while the error content is included in the non-periodic terms.

Accordingly, the unmodelled non-periodic components and observation errors can be handled independently from the annual component, and the later component can be described by an error of 2.49% of the signal content due to the sampling and an error of 1.15% of the signal content due to the averaging.

Example in the space domain: the Hungarian Gravimetric Network

In order to indicate the relevance of the errors contaminated by the sampling, a case study of the comparison of two epochs of the Hungarian Gravimetric Network (MGH) is provided. The first epoch of the network was dated to the 1950s, labelled as MGH-50 (Facsinay-Szilárd, 1956), while the second one is dated to 2000, referred to as MGH-2000 (Csapó, 2000). The distribution of the gravimetric stations is shown in Figure 6 for the MGH-50 and the MGH-2000 networks.

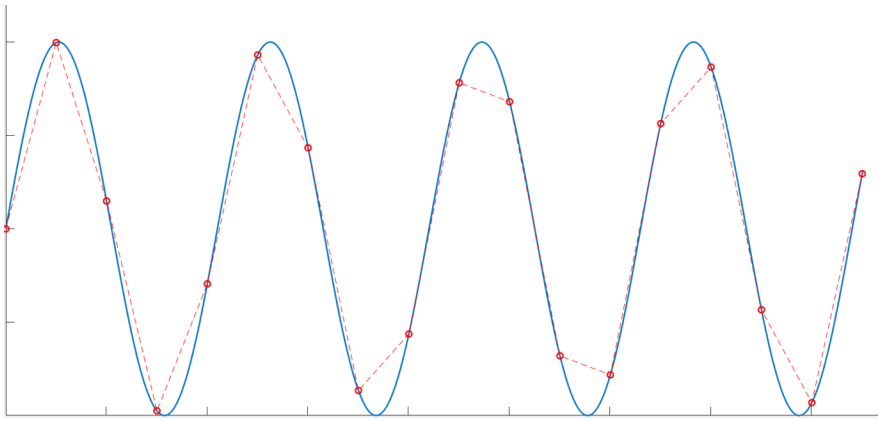


Figure 6. The point distribution of the MGH-50 and MGH-2000 gravimetric network

The covered area (the area of the country) is approximately 93000 km^2, the number of stations is more than 900 for both the MGH-50 and the MGH-2000 networks, the gravity interval of the country is approximately 350 mGal. The distance between gravimetric stations is roughly 10 km, thus it provides a nice coverage of the country for capturing the relevant features of the gravity field.

For historical reasons, however, most stations of the MGH-50 network have been perished, accordingly, most points of the MGH-2000 are newly established stations. In fact, there are only 13 identical stations of the two networks (see common points in Figure 6). Apart from the change of the gravity by time (which is not striking due to the moderate tectonics of the area), the two networks are meant to present two independent description of the same phenomenon, that is the gravity field of Hungary.

Based on the gravity values of MGH-50 and MGH-2000 networks, gravity has been interpolated onto a common grid, and the difference of the two grids is displayed in Figure 7. Even though the difference between them is in the range of some mGals, there are striking outliers reaching even the 100 mGal value. This is very much, which cannot be interpreted neither with the temporal variations of the gravity field nor with observation errors. This difference is obviously a consequence of the different sampling of the gravity field.

Posted on Authorea 4 Aug 2020 — The copyright holder is the author/funder. All rights reserved. No reuse without permission. — https://doi.org/10.22541/au.159654396.62738949 — This a preprint and has not been peer reviewed. Data may be preliminary.

Posted on Authorea 4 Aug 2020 — The copyright holder is the author/funder. All rights reserved. No reuse without permission. — https://doi.org/10.22541/au.159654396.62738949 — This a preprint and has not been peer reviewed. Data may be preliminary.

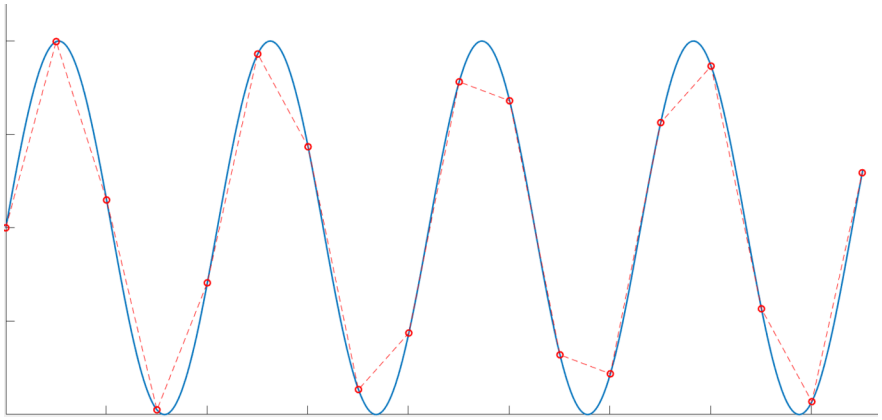


Figure 7. Differences of interpolated gravity fields based on MGH-50 and on MGH-2000 gravimetric network data. The values of the colourbar are in mGal unit.

Using the formulations above, the adequacy of the resolution of the Hungarian gravity network can be tested. According to equation (15), with stations located about 10 km distance from each other, features of the gravity field can be observed with 5%, 1% and 0.1% sampling error up to a resolution of 0.18 km, 0.42 km and 1.33 km, respectively. Indeed, local gravity anomalies can be relevant with even finer resolutions, therefore it is obvious that the 10 km distance between the stations are capable only for capturing middle wavelength gravity field variations.

A more reliable and informative test can be provided if also the magnitude of the observable is considered. Since the gravity field sums up of gravity features at different scales (ranging from local to global), the spectral behaviour of the gravity field should be modelled. In our case it is approximated by the Kaula's rule of thumb (Kaula 1966), which is expressed in equation (31) for gravity anomaly, g:

$\sigma(g) = \frac{\mathrm{kM}}{R^2}(n-1) \bullet \frac{\sqrt{2n+1}}{n^2} 10^{-5}$ (31).

The Kaula's rule of thumb estimates the signal content of gravity as a function of the spherical harmonic degree, n, for an Earth with an average mass M and an average radius R. The 'classical' rule of thumb (referring to the potential) is converted to gravity anomaly,g by multiplying it with the transfer function of the spherical harmonic expansion of the gravity anomaly. (For detailed explanation on the physical content of the Kaula's rule of thumb see Kaula (1992), Rummel (2004) and McMahon et al. (2016)).

The spherical harmonic degree, n can approximately be related to the scale of the gravity content, i.e. to the spatial resolution of the features of the gravity field (described by a wavelength T).

$T(g) = \frac{2\pi R}{n}$ (32).

Using (31) and (32), Figure 8 shows an estimate of the gravity field content by the spatial resolution according to Kaula's rule of thumb in logarithmic scale. In the discussion below, two terms highly used in geodesy are applied here. These are: omission error refers to those errors, which are committed due to omitting certain parts of the frequency spectrum, while commission error refers to the errors provided by the involved frequencies. Certainly, the total error is a combination of the omission and commission errors, and one can only attempt to separate them based on the spatial resolution of the observed total error.

Posted on Authorea 4 Aug 2020 — The copyright holder is the author/funder. All rights reserved. No reuse without permission. — https://doi.org/10.22541/au.159654396.62738949 — This a preprint and has not been peer reviewed. Data may be preliminary.

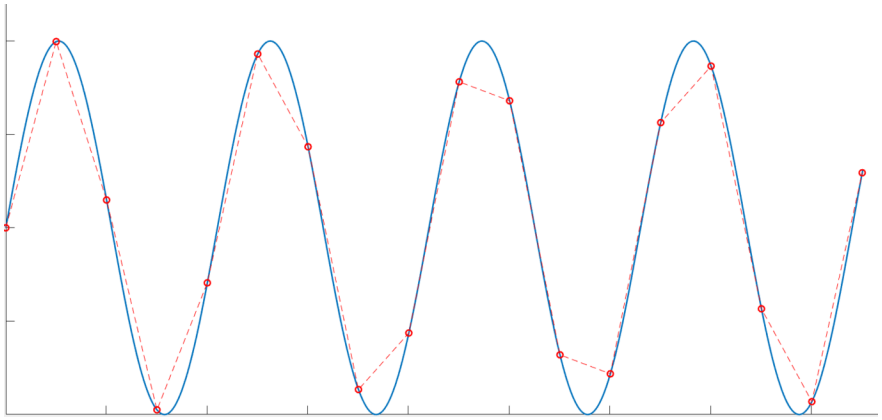


Figure 8. Signal content of gravity anomaly based on Kaula's rule of thumb vs. sampling error (by L1-norm and L2-norm as well) according to a sampling rate, T of 10 km.

The sampling error is estimated by L1-norm and L2-norm using equation (15). The value of the sampling rate has been set to $T = 10km$, and the values of N were determined by using T as the independent variable. The resulted curves are shown in Figure 8. The maximal value of N was 0.5 according to the Nyquist criterion, which is at the distance of 20 km. The $N = 1$ abscissa is displayed on the figure by a vertical dotted line, which refers to the $T = T = 10km$ value. By any mean, signal content below $T = 10km$ appears as noise in the signal, as the corresponding frequencies are overlooked (not sampled) by the $T = 10km$ sampling rate. The omission of the signal content of the short wavelength gravity (i.e. at less than $10km$ resolution) may particularly be relevant at mountainous regions, where the gravity may change more sharply, the gradients of the gravity are larger. Basically, omission error of the short wavelength gravity is the primer source of 100 mGal large, very localized outliers in Figure 7.

Beyond the omission error, the commission error due to the sampling is also large: according to Figure 8, the sampling generated error reaches the signal at 28.1 km (L1-norm) and 26.8 km (L2-norm). A signal is reliable up to that point where its noise content is at least one order of magnitude smaller than the signal content, i.e. the Signal-to-Noise ratio is 10. In the case of Figure 8, this is reached at 73.8 km (L1-norm) and 70.7 km (L2-norm), so any smaller scale gravity information can be gained only quite uncertainly due to the commission error. As in an actual case both the omission and commission errors affect the solution, the gravity field with 10 km sampling may describe properly the gravity field features up to 100 km resolution only.

Summary

Sampling of continuous signals cannot be avoided for practical applications therefore sampling errors are contaminating the knowledge of the continuous signal. In order to check whether the sampling is sufficiently fine for a certain application, a simple test on the sampling rate can be performed. In this study, analytic formulation for L1-norm sampling error estimate of a periodic signal has been delivered in a closed form. Also, the L2-norm error estimate has been derived making use of a symbolic programming module of Matlab, which has not been presented here but applied for the tests. According to the results, the 5%, 1% and 0.1% errors can be reached by N=0.177, 0.078 and 0.025, equivalent to 6, 13 and 41 samples per period, respectively.

As an example, GRACE-borne gravity anomaly time series are analysed for the region of the Amazonas basin. It was found that the unmodelled non-periodic components and observation errors can be handled independently from the annual component, and that the annual component can be described by an error of 2.49% of the signal content due to the sampling and an error of 1.15% of the signal content due to the averaging.

As a spatial example, the case of the Hungarian gravity network is analysed. With stations located about

Posted on Authorea 4 Aug 2020 — The copyright holder is the author/funder. All rights reserved. No reuse without permission. — https://doi.org/10.22541/au.159654396.62738949 — This a preprint and has not been peer reviewed. Data may be preliminary.

10 km distance from each other, both omission and commission errors were found to be relevant. Fine features of the gravity field are largely contaminated by the omission of the gravity signal over less than 10 km scales, resulting in huge, local peaks in the gravity anomaly error map in Figure 6. Commission error was found to be relevant up to a resolution of approximately 70 km. As in an actual case both the omission and commission errors affect the solution, the gravity field with 10 km sampling may describe properly the gravity field features up to 100 km resolution only. For reducing the spatial resolution, the sampling density should be increased further.

References

1. Benedetto, J. J. (1992): Irregular sampling and frames, in: Wavelets - A Tutorial in Theory and Applications, C.K. Chui (Ed.), Boca Raton, FL, CRC Press, pp. 445–507.
2. Bettadpur, S. (2007): Gravity Recovery and Climate Experiment Level-2 Gravity Field Product User Handbook, GRACE 327-734, CSR Publ. GR-03-01, Rev 2.3, pp. 19, University of Texas at Austin, USA.
3. Csapó, G. (2000): The Hungarian Gravimetric Network, MGH-2000 (In Hungarian; Magyarország új gravimetriai alaphálózata, MGH–2000), Geodézia és Kartográfia, 52(2), p. 27-33.
4. Duffin, R. J., Schaeffer, A. C. (1992): A class of nonharmonic Fourier series, Trans. Amer. Math. Soc., vol. 72, pp. 314–366.
5. Facsinay L., Szilárd J. (1956): The Hungarian Gravimetric Network (in Hungarian; A magyar országos gravitációs hálózat), Geofizikai Közlemények, V(2), p. 3-49.
6. Földváry, L (2015).: Desmoothing of averaged periodical signals for geodetic applications, Geophysical Journal International, 201 (3): 1235-1250, DOI 10.1093/gji/ggv092
7. Kaula, W, M. (1966): Theory of Satellite Geodesy, Blaisdell, Waltham
8. Kaula W.M. (1992): Properties of the Gravity Fields of Terrestrial Planets. In: Colombo O.L. (ed.) From Mars to Greenland: Charting Gravity With Space and Airborne Instruments. International Association of Geodesy Symposia, vol 110. Springer, New York, NY, 1-10.
9. Leis, J. W. (2011): Digital Signal Processing Using MATLAB for Students and Researchers. John Wiley & Sons. p. 82, ISBN 9781118033807
10. Mallat, S. (1998): A Wavelet Tour of Signal Processing. San Diego, CA, Academic.
11. Marks, R.J. (1991): Introduction to Shannon Sampling and Interpolation Theory, Springer-Verlag
12. Marks, R.J., editor (1993): Advanced Topics in Shannon Sampling and Interpolation Theory, Springer-Verlag
13. McMahon, J. W., Farnocchia, D., Scheeres, D., Chesley, S. (2016): Understanding Kaula's Rule for Small Bodies, 47th Lunar and Planetary Science Conference 2016, paper 2129.
14. Rummel, R. (2004): Gravity and Topography of Moon and Planets. Earth Moon Planet 94, 103–111. https://doi.org/10.1007/s11038-005-3245-z
15. Selesnick, I. W. (1999): Interpolating multiwavelets bases and the sampling theorem, IEEE Trans. Signal Processing, vol. 47, no. 6, pp. 1615–1621.
16. Shannon, C. E. (1949): Communication in the presence of noise, in: Proc. IRE, vol. 37, pp. 10-21.
17. Shannon, C. E. (1998): Classic paper: Communication in the presence of noise, Proc. IEEE, vol. 86, no. 2, pp. 447–457.
18. Strang, G. (1971): The finite element method and approximation theory, in: Numerical Solution of Partial Differential Equations—II, B. Hubbard (Ed.), New York, Academic, pp. 547–583.
19. Strang, G., Nguyen, T. (1996): Wavelets and Filter Banks. Wellesley, MA, Wellesley-Cambridge.
20. Swenson, S., J. Wahr, and P. C. D. Milly (2003): Estimated accuracies of regional water storage variations inferred from the gravity recovery and climate experiment (GRACE), Water Resources Research, 39, 11–1. https://doi.org/10.1029/2002WR001808
21. Unser, M. (2000): Sampling-50 Years after Shannon, Proc. IEEE, 88(4), p. 569–587.
22. Wahr, J., S. Swenson, and I. Velicogna (2006), Accuracy of GRACE mass estimates, Geophysical Research Letteres, 33, L06,401, doi:10.1029/2005GL025305.

Appendix A

Posted on Authorea 4 Aug 2020 — The copyright holder is the author/funder. All rights reserved. No reuse without permission. — https://doi.org/10.22541/au.159654396.62738949 — This a preprint and has not been peer reviewed. Data may be preliminary.

According to equation (8), a closed-form for the L1-norm can be derived by solving equation (7), which reads

$$\sigma_{L1}\left([x_i, x_{i+1}]\right) = \frac{\int_{x_i}^{x_{i+1}} \left| Asin(2\pi\omega\ x+\phi) - \frac{(x_{i+1}-x)Asin(2\pi\omega\ x_i+\phi)+(x-x_i)Asin(2\pi\omega\ x_{i+1}+\phi)}{T} \right| \mathrm{dx}}{T} \text{(A1)}.$$

Concentrating on the integration in the numerator, there are two integrations should be completed, since

$L1\left(|\varepsilon|\right) = L1\left(\varepsilon\right)$ or $L1\left(|\varepsilon|\right) = L1\left(-\varepsilon\right)$ (A2).

In the$L1\left(|\varepsilon|\right) = L1\left(\varepsilon\right)$case the derivation starts with splitting the integrand into separated terms,

$$\int_{x_i}^{x_{i+1}} \left(Asin(2\pi\omega\ x+\phi) - \frac{(x_{i+1}-x)Asin(2\pi\omega\ x_i+\phi)+(x-x_i)Asin(2\pi\omega\ x_{i+1}+\phi)}{T} \right) \mathrm{dx} = \int_{x_i}^{x_{i+1}} A\sin\left(2\pi\omega\ x+\phi\right) \mathrm{dx} - \int_{x_i}^{x_{i+1}} \frac{x_{i+1}\,\mathrm{Asin}(2\pi\omega\ x_i+\phi)}{T} \mathrm{dx} + \int_{x_i}^{x_{i+1}} \frac{\mathrm{Asin}(2\pi\omega\ x_i+\phi)}{T} \mathrm{xdx} - \int_{x_i}^{x_{i+1}} \frac{\mathrm{Asin}(2\pi\omega\ x_{i+1}+\phi)}{T} \mathrm{xdx} + \int_{x_i}^{x_{i+1}} \frac{x_i\,\mathrm{Asin}(2\pi\omega\ x_{i+1}+\phi)}{T} \mathrm{dx} \text{(A3)}.$$

By performing the definite integration, and making use of

$x_{i+1} = x_i + \mathrm{T}$ (A4),

equation (A3) becomes

$$\left[-\frac{A}{2\pi\omega}\cos\left(2\pi\omega\ x+\phi\right)\right]_{x_i}^{x_{i+1}} - \left[\frac{x_{i+1}\,\mathrm{Asin}(2\pi\omega\ x_i+\phi)}{T} x\right]_{x_i}^{x_{i+1}} + \left[\frac{\mathrm{Asin}(2\pi\omega\ x_i+\phi)}{T}\frac{x^2}{2}\right]_{x_i}^{x_{i+1}} - \left[\frac{\mathrm{Asin}(2\pi\omega\ x_{i+1}+\phi)}{T}\frac{x^2}{2}\right]_{x_i}^{x_{i+1}} + \left[\frac{x_i\,\mathrm{Asin}(2\pi\omega\ x_{i+1}+\phi)}{T} x\right]_{x_i}^{x_{i+1}} = -\left(\frac{A}{2\pi\omega}\cos\left(2\pi\omega\ x_i+2\pi\omega\ T+\phi\right) - \frac{A}{2\pi\omega}\cos\left(2\pi\omega\ x_i+\phi\right)\right) - (x_i+T)\,\mathrm{Asin}\left(2\pi\omega\ x_i+\phi\right) + \mathrm{Asin}\left(2\pi\omega\ x_i+\phi\right)\left(x_i+\frac{T}{2}\right) - \mathrm{Asin}\left(2\pi\omega\ x_i+2\pi\omega\ T+\phi\right)\left(x_i+\frac{T}{2}\right) + x_i\,\mathrm{Asin}\left(2\pi\omega\ x_i+2\pi\omega\ T+\phi\right) = -\frac{A}{2\pi\omega}\cos\left(2\pi\omega\ x_i+2\pi\omega\ T+\phi\right) + \frac{A}{2\pi\omega}\cos\left(2\pi\omega\ x_i+\phi\right) - \frac{T}{2}\,\mathrm{Asin}\left(2\pi\omega\ x_i+\phi\right) - \frac{T}{2}\,\mathrm{Asin}\left(2\pi\omega\ x_i+2\pi\omega\ T+\phi\right) \text{(A5)}.$$

Applying trigonometric identities

$\cos\left(\alpha+\beta\right) = \cos\alpha\cos\beta - \sin\alpha\sin\beta$ (A6)

and

$\sin\left(\alpha+\beta\right) = \sin\alpha\cos\beta + \cos\alpha\sin\beta$ (A7),

equation (A5) is reformulated as

$$-\frac{A}{2\pi\omega}\left(\cos\left(2\pi\omega\ x_i+\phi\right)\cos\left(2\pi\omega\ T\right) - \sin\left(2\pi\omega\ x_i+\phi\right)\sin\left(2\pi\omega\ T\right)\right) + \frac{A}{2\pi\omega}\cos\left(2\pi\omega\ x_i+\phi\right) - \frac{T}{2}\,\mathrm{Asin}\left(2\pi\omega\ x_i+\phi\right) - \frac{T}{2}A\left(\sin\left(2\pi\omega\ x_i+\phi\right)\cos\left(2\pi\omega\ T\right) + \cos\left(2\pi\omega\ x_i+\phi\right)\sin\left(2\pi\omega\ T\right)\right) = -\frac{A}{2\pi\omega}\cos\left(2\pi\omega\ T\right)\cos\left(2\pi\omega\ x_i+\phi\right) + \frac{A}{2\pi\omega}\sin\left(2\pi\omega\ T\right)\sin\left(2\pi\omega\ x_i+\phi\right) + \frac{A}{2\pi\omega}\cos\left(2\pi\omega\ x_i+\phi\right) - A\frac{T}{2}\sin\left(2\pi\omega\ x_i+\phi\right) - A\frac{T}{2}\cos\left(2\pi\omega\ T\right)\sin\left(2\pi\omega\ x_i+\phi\right) - A\frac{T}{2}\sin\left(2\pi\omega\ T\right)\cos\left(2\pi\omega\ x_i+\phi\right) = \left(-\frac{A}{2\pi\omega}\cos\left(2\pi\omega\ T\right) + \frac{A}{2\pi\omega} - A\frac{T}{2}\sin\left(2\pi\omega\ T\right)\right)\cos\left(2\pi\omega\ x_i+\phi\right) + \left(\frac{A}{2\pi\omega}\sin\left(2\pi\omega\ T\right) - A\frac{T}{2} + A\frac{T}{2}\cos\left(2\pi\omega\ T\right)\right)\sin\left(2\pi\omega\ x_i+\phi\right)\text{(A}$$

Inserting (A8) to the numerator of (A1), it becomes

$$\sigma_{L1}\left([x_i, x_{i+1}]\right) = \left(-\frac{A}{2\pi\omega T}\cos\left(2\pi\omega\ T\right) + \frac{A}{2\pi\omega T} - \frac{A}{2}\sin\left(2\pi\omega\ T\right)\right)\cos\left(2\pi\omega\ x_i+\phi\right) + \left(\frac{A}{2\pi\omega T}\sin\left(2\pi\omega\ T\right) - \frac{A}{2} + \frac{A}{2}\cos\left(2\pi\omega\ T\right)\right)\sin\left(2\pi\omega\ x_i+\phi\right)\text{(A9)},$$

Now let's see the$L1\left(|\varepsilon|\right) = L1\left(-\varepsilon\right)$case. In this integrand, similarly to (A3) becomes

$$\int_{x_i}^{x_{i+1}} \left(\frac{(x_{i+1}-x)Asin(2\pi\omega\ x_i+\phi)+(x-x_i)Asin(2\pi\omega\ x_{i+1}+\phi)}{T} - Asin(2\pi\omega\ x+\phi) \right) \mathrm{dx}\text{(A10)},$$

so only the sign of the two main terms is exchanged. The derivation using the steps through (A3) to (A9) are identical apart from the consequent change of the sign, resulting in

$$\sigma_{L1}\left([x_i, x_{i+1}]\right) = \left(\frac{A}{2\pi\omega T}\cos\left(2\pi\omega\ T\right) - \frac{A}{2\pi\omega T} + \frac{A}{2}\sin\left(2\pi\omega\ T\right)\right)\cos\left(2\pi\omega\ x_i+\phi\right) + \left(-\frac{A}{2\pi\omega T}\sin\left(2\pi\omega\ T\right) + \frac{A}{2} - \frac{A}{2}\cos\left(2\pi\omega\ T\right)\right)\sin\left(2\pi\omega\ x_i+\phi\right)\text{(A11)},$$

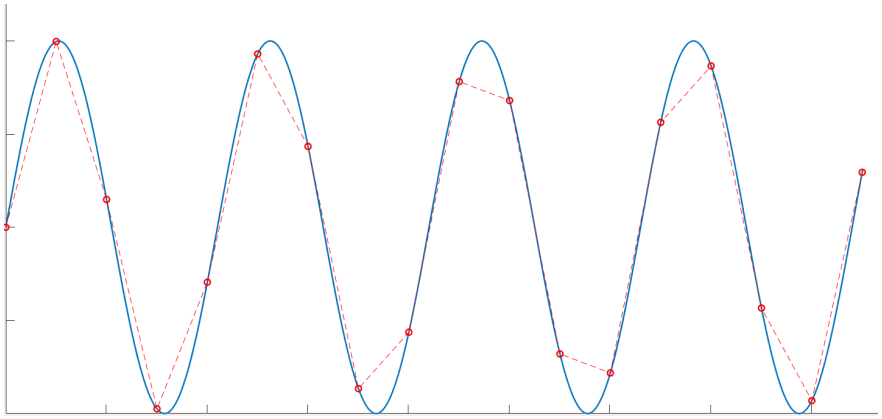
Posted on Authorea 4 Aug 2020 — The copyright holder is the author/funder. All rights reserved. No reuse without permission. — https://doi.org/10.22541/au.159654396.62738949 — This a preprint and has not been peer reviewed. Data may be preliminary.

which is the same as (A9) apart from the opposite sign of the coefficients of the sine and cosine functions of$2\pi\omega\ x_i + \phi$.

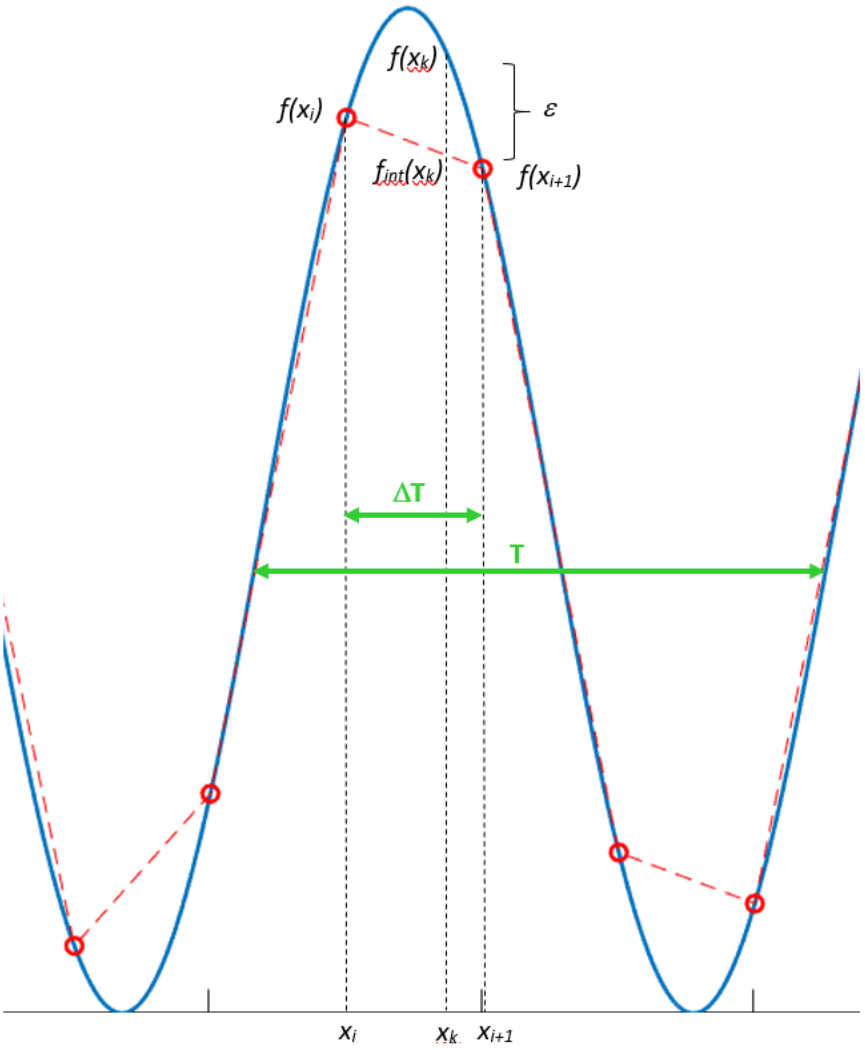
Equations (A9) and (A11) provides a solution in a form of

$\sigma_{L1}\left([x_i, x_{i+1}]\right) = C \bullet \cos\left(2\pi\omega x_i + \phi\right) + S \bullet sin(2\pi\omega x_i + \phi)$(A12).

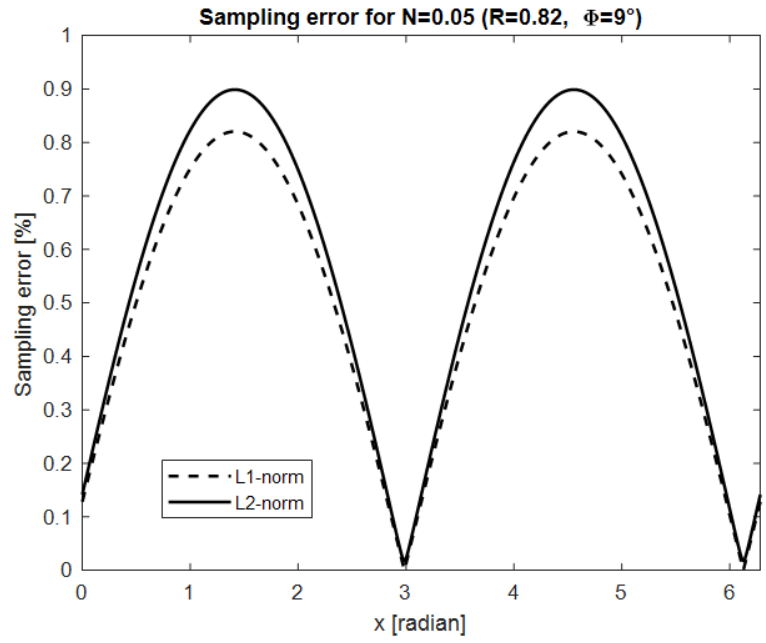
By generalizing the solutions (A9) and (A11) in the form of (8) instead of (A12), they are equivalent to equation (8) to (10) of the article.

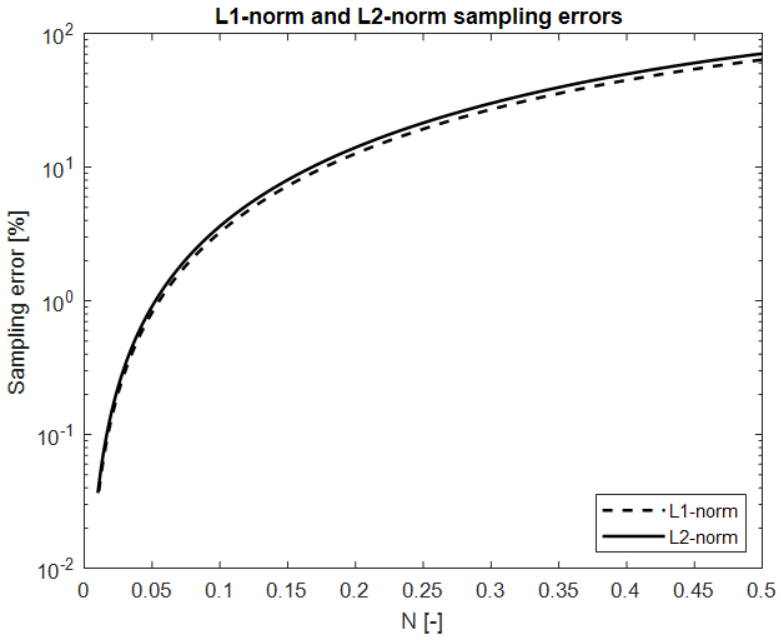


Posted on Authorea 4 Aug 2020 — The copyright holder is the author/funder. All rights reserved. No reuse without permission. — https://doi.org/10.22541/au.159654396.62738949 — This a preprint and has not been peer reviewed. Data may be preliminary.

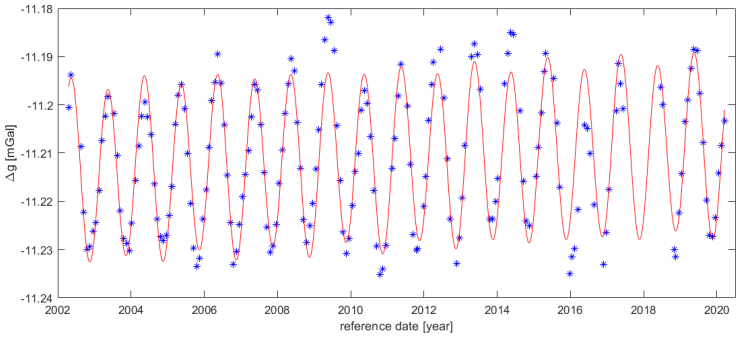


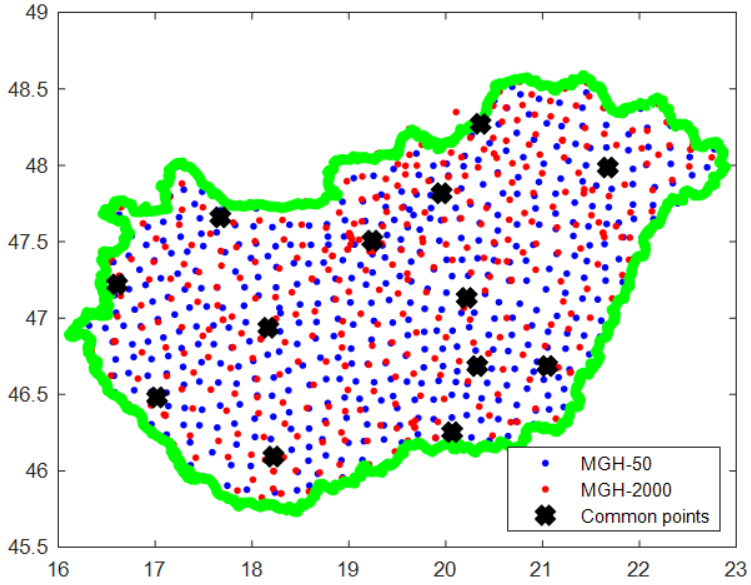
Posted on Authorea 4 Aug 2020 — The copyright holder is the author/funder. All rights reserved. No reuse without permission. — https://doi.org/10.22541/au.159654396.62738949 — This a preprint and has not been peer reviewed. Data may be preliminary.





Posted on Authorea 4 Aug 2020 — The copyright holder is the author/funder. All rights reserved. No reuse without permission. — https://doi.org/10.22541/au.159654396.62738949 — This a preprint and has not been peer reviewed. Data may be preliminary.





Posted on Authorea 4 Aug 2020 — The copyright holder is the author/funder. All rights reserved. No reuse without permission. — https://doi.org/10.22541/au.159654396.62738949 — This a preprint and has not been peer reviewed. Data may be preliminary.

